Dynamic Article Links

Organic & Biomolecular Chemistry

Cite this: *Org. Biomol. Chem.*, 2011, **9**, 8356

www.rsc.org/obc

PAPER

Synthesis of a library of oligothiophenes and their utilization as fluorescent ligands for spectral assignment of protein aggregates†

Therése Klingstedt, Andreas Åslund, Rozalyn A. Simon, Leif B. G. Johansson, Jeffrey J. Mason, Sofie Nyström, Per Hammarström and K. Peter R. Nilsson*

Received 21st April 2011, Accepted 23rd September 2011
DOI: 10.1039/c1ob05637a

Molecular probes for selective identification of protein aggregates are important to advance our understanding of the molecular pathogenesis underlying protein aggregation diseases. Here we report the chemical design of a library of anionic luminescent conjugated oligothiophenes (LCOs), which can be utilized as ligands for detection of protein aggregates. Certain molecular requirements were shown to be necessary for detecting (i) early non-thioflavinophilic protein assemblies of Aβ1-42 and insulin preceding the formation of amyloid fibrils and (ii) for obtaining distinct spectral signatures of the two main pathological hallmarks observed in human Alzheimer's diease brain tissue (Aβ plaques and neurofibrillary tangles). Our findings suggest that a superior anionic LCO-based ligand should have a backbone consisting of five to seven thiophene units and carboxyl groups extending the conjugated thiophene backbone. Such LCOs will be highly useful for studying the underlying molecular events of protein aggregation diseases and could also be utilized for the development of novel diagnostic tools for these diseases.

Introduction

The development of molecular probes for the detection of proteinaceous deposits is of great importance, as the formation of extra- or intracellular protein aggregates is the common pathological hallmark associated with many diseases, including Alzheimer's, Parkinson's and Huntington's disease, and the infectious prion diseases.[1] From an ultrastructural perspective, these protein deposits consist mainly of amyloid fibrils with a diameter of 7–10 nm[2–4] and the detection of these species has for several decades relied on small hydrophobic dyes, such as derivatives of Congo red (CR)[5–7] and Thioflavin T (ThT).[8–10] These ligands do not bind to specific proteins but are rather selective towards protein aggregates having an extensive cross β-pleated sheet conformation and a structural regularity,[6,11] the typical molecular characteristics of presumably all amyloid fibrils.[12,13] The affinity of CR with a resulting yellow-green birefringence is one of the amyloid criteria,[14] but the specificity of CR has been questioned.[15,16] The information that can be obtained from these conventional probes is also somewhat limited and they cannot be utilized to characterize various conformational entities, such as pre-fibrillar species or heterogenic populations of protein aggregates. It is evident that significant morphological variation can exist between different amyloid fibrils formed from the same peptide or protein and that pre-fibrillar states preceding the formation of well-defined amyloid fibrils are likely to play a critical role in the pathogenesis of protein aggregation diseases.[17–19]

ThT and CR have also shown limitations for detecting disease associated protein aggregates in tissue samples and recently we introduced luminescent conjugated polythiophenes (LCPs) as a novel class of fluorescent probes for the detection of protein aggregates.[20–25] In 2009, Åslund *et al.*[26] improved the concept and presented defined pentameric structures termed luminescent conjugated oligothiophenes (LCOs) that could be utilized for *in vivo* imaging of protein aggregates. In comparison with conventional amyloid ligands, LCPs and LCOs have a conjugated thiophene backbone, which brings about a connection between the conformation of the thiophene backbone and its spectral properties.[22,27] When binding to protein aggregates, the conformation of the backbone is dictated by the protein, which results in conformation-sensitive spectral signatures from the LCP or LCO.[28] LCPs and LCOs have been utilized for staining of thioflavinophilic and congophilic protein aggregates associated with a variety of diseases[21–26] and also for identifying disease-associated protein aggregates that go undetected with ThT and CR.[23,26,29–34] For instance, LCPs and LCOs have proven very useful for identification of protein aggregates associated with distinct prion strains[26,29,31] and for staining of intracelllular inclusion bodies.[34]

Staining of brain sections from Alzheimer's disease (AD) patients with the anionic LCO p-FTAA has revealed a spectral discrimination between the two classical pathological hallmarks of AD, amyloid β (Aβ) plaques and neurofibrillary tangles (NFTs)

Department of Chemistry, Linköping University, SE-581 83 Linköping, Sweden. E-mail: petni@ifm.liu.se; Tel: +46 13 28 27 87

† Electronic supplementary information (ESI) available: Supplementary Fig. 1, supplementary Table 1 and NMR spectra. See DOI: 10.1039/c1ob05637a

formed of hyperphosphorylated tau protein. Interestingly, this phenomenon was lost when the carboxyl groups were removed from the 2- or 5′′′′-positions of the p-FTAA backbone. The spectral distinction was also abolished when the thiophene backbone was extended and more negatively charged groups were added.[26] Therefore, we now wanted to investigate how the carboxyl groups and various lengths of the thiophene backbone influence the observed spectral difference between Aβ plaques and NFTs.

Furthermore, we also wanted to examine if the capacity to detect non-thioflavinophilic protein assemblies preceding the formation of amyloid fibrils, as recently reported for p-FTAA,[35] is affected by changing the chemical composition of the LCOs. Herein we report the synthesis of a novel set of anionic oligothiophene probes and the utilization of this library to provide further insight of the basic molecular requirements for achieving an optimal performance of these molecules as ligands for spectral assignment of protein aggregates.

Results and discussion

Synthesis of luminescent conjugated oligothiophenes

To investigate if and how the length of the thiophene backbone and different chemical substituents affect the performance of LCOs, we synthesized a library of nine LCOs with backbone lengths varying from four to seven thiophenes and with end thiophenes substituted with hydrogen or carboxyl groups at the α-position (Fig. 1 and Fig. 2). The synthesis of the thiophene trimer (**10**) and the three pentameric oligothiophenes, **15**, p-HTAA (**4**) and p-FTAA (**5**) have been reported previously.[26,36] The thiophene trimer **10** is the starting point for the synthesis of tetramers q-HTAA (**2**) and q-FTAA (**3**), pentamers p-HTAA (**4**) and p-FTAA (**5**), and heptamers h-HTAA (**8**) and h-FTAA (**9**) (Scheme 1). Tetrathiophene **19** on the other hand serves as the core building block for tetramer t-HTAA (**1**) and hexamers hx-HTAA (**6**) and hx-FTAA (**7**) (Scheme 2). As mentioned above, the LCOs are also varied by having hydrogen or carboxyl groups at the end α-positions of the LCOs. These different variants are referred to as "H"-variants (**1**, **2**, **4**, **6** and **8**) for the hydrogen-substituted ones and "F"-variants (**3**, **5**, **7** and **9**) for the carboxyl-substituted ones. **10** was mono-brominated using *N*-bromosuccinimide (NBS) in DMF at −15 °C giving product **11** in 70% yield. The two α-positions of **10** are equal in reactivity as the reaction starts. However, when the first α-position has reacted, the reactivity of the second α-position drops. Hence, a yield above the statistical 50% can be afforded. The mixture of unreacted starting material, mono-brominated product and di-brominated product was purified by reversed phase. Two other bromination reactions were used during the synthesis. The bromination of thiophene acetic acid gave an acceptable yield (60%) of **18**. Position 2 is more reactive as the intermediate carbocation in position 3 becomes stabilized by the side chain during the reaction. The last bromination performed was the di-bromination of oligothiophenes **15** and **19**, this reaction was rather easy as both α-positions should react, but one should be careful not to over-brominate the compound. The coupling of brominated oligothiophenes **11**, **16**, **18** and **20** with the appropriate boronic acid or boronic ester was performed using Suzuki cross coupling conditions with the commercially available PEPPSI-IPr as Pd-catalyst and potassium carbonate as base. This gave the products **12**, **13**, **14**, **17**, **19**, **21** and **22** in 80–99% yield. Lastly, all methylesters (**12**, **13**, **14**, **17**, **19**, **21** and **22**) were hydrolyzed in dioxane using 1.5 equiv. of sodium hydroxide per ester and acid on the starting material. Once precipitation started, water was added to the reaction to dissolve the product. After completion, the products **1**, **2**, **3**, **6**, **7**, **8**, **9** were lyophilized and used without further purification. The LCOs and all precursor molecules were verified with ^{1}H and ^{13}C NMR, IR, and UV/Vis absorbance (see the ESI†). However, due to their rather extensive backbones, compounds **14**, **17** and **22** probably form rather large complexes in most solvents. Therefore, we achieved less resolved NMR spectra of these three compounds, compared to the other molecules.

Fibrillation of Aβ1-42 and insulin monitored by LCOs

To verify selective binding of the LCOs to protein aggregates, we screened all nine LCOs against ThT positive amyloid fibrils made from recombinant Aβ1-42 peptide. All of the LCOs revealed well-resolved excitation and emission spectra with typical shifts in wavelengths when binding to recombinant Aβ fibrils (Fig. 1, Fig. 2 and Table S1†). These significant changes in the spectral profiles were not seen for LCOs in buffer solution or when mixed with freshly dissolved Aβ1-42. The enhanced emission and the well-resolved spectral substructures most likely arise from a conformationally restricted thiophene backbone,[37,38] due to selective interactions with the Aβ fibrils.

The pronounced shifts (around 50 nm) of the excitation spectra towards longer wavelengths indicate that the LCOs adopt a more extended conformation upon binding to the amyloid fibril resulting in a larger transition dipole moment along the conjugated molecular framework. A variety of studies suggest that other amyloid ligands bind in grooves along the long axis of the amyloid fibril.[11,39–41] LCOs are presumably intercalating with the amyloid fibrils through a similar mechanism[42] and the constraints of the fibril binding pocket are inducing unique excitation and emission pathways for the LCO. Hence, the nine LCOs provide distinct optical signatures upon binding to Aβ1-42 fibrils (Fig. 1 and Fig. 2).

The development of tools able to identify species preceding the final fibrillar state has lately emerged as crucial, since there is an increasing awareness of these pre-fibrillar species playing an important role in the pathogenesis of misfolding diseases.[17–19] Recently, Jovin and co-workers[43] presented an ESIPT (excited-state intramolecular proton transfer) probe sensitive to early and intermediate stages of α-synuclein aggregation and the pentameric LCO p-FTAA was recently reported[26,35] to detect early non-thioflavinophilic species occurring during the fibrillation pathway of several amyloidogenic proteins. Therefore, we next utilized the library of LCOs for monitoring the kinetics of recombinant Aβ1-42 fibrillation *in situ*. As we were not able to identify pre-fibrillar species with transmission electron microscopy (TEM) or p-FTAA utilizing our previously reported protocol for Aβ1-42 fibrillation,[26] we tried different fibrillation protocols to achieve reproducible fibrillation kinetics of Aβ1-42 having a prolonged lag phase offering the possibility to observe pre-fibrillar states preceding the formation of amyloid fibrils. The conditions identified were close to physiological (37 °C, 10 mM phosphate buffer supplemented with 140 mM NaCl and 2.7 mM KCl pH 7.4, quiescent) and the concentration of probe was well below the one used for Aβ (0.3 μM probe and 10 μM Aβ peptide, respectively). When the

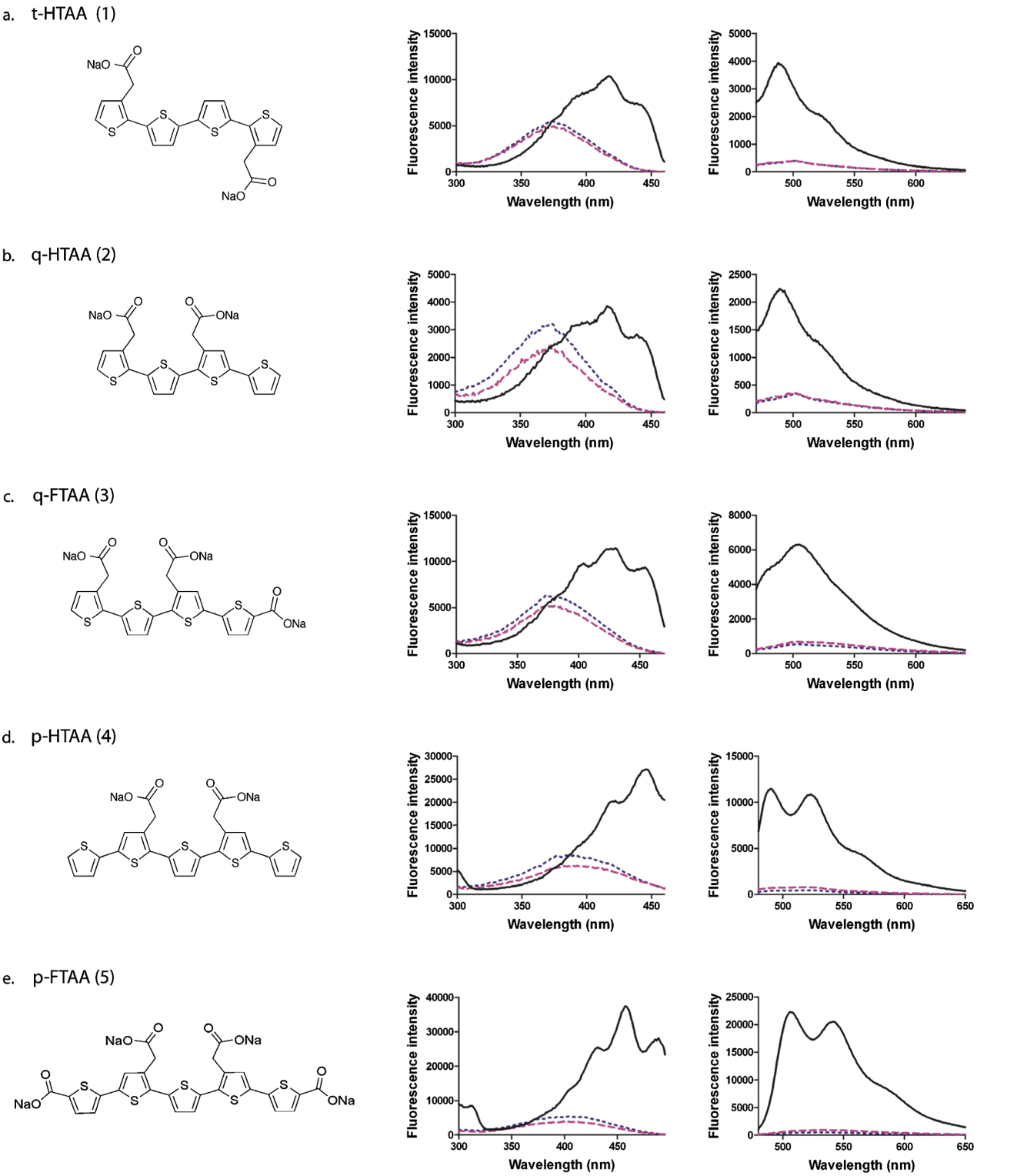

Fig. 1 Chemical structure (left panel), excitation spectrum (middle panel) and emission spectrum (right panel) of t-HTAA (a), q-HTAA (b), q-FTAA (c), p-HTAA (d) and p-FTAA (e). The spectral graphs display excitation/emission spectra of the different LCOs in PBS (blue dotted line), in PBS with soluble Aβ1-42 (magenta dashed line) or in PBS with fibrillar Aβ1-42 (black solid line). The excitation/emission wavelengths were 430/490 nm for t-HTAA, 430/490 nm for q-HTAA, 430/505 nm for q-FTAA, 450/490 nm for p-HTAA and 450/507 nm for p-FTAA. All probes show well-resolved excitation and emission spectra when binding to Aβ fibrils.

fluorescence intensity was plotted against time it became evident that a LCO backbone consisting of five or more thiophenes is a prerequisite for detecting non-thioflavinophilic species preceding mature fibrils in the Aβ fibrillation pathway (Fig. 3). Interestingly, the main difference between the fibrillation protocol reported herein compared to our previously reported

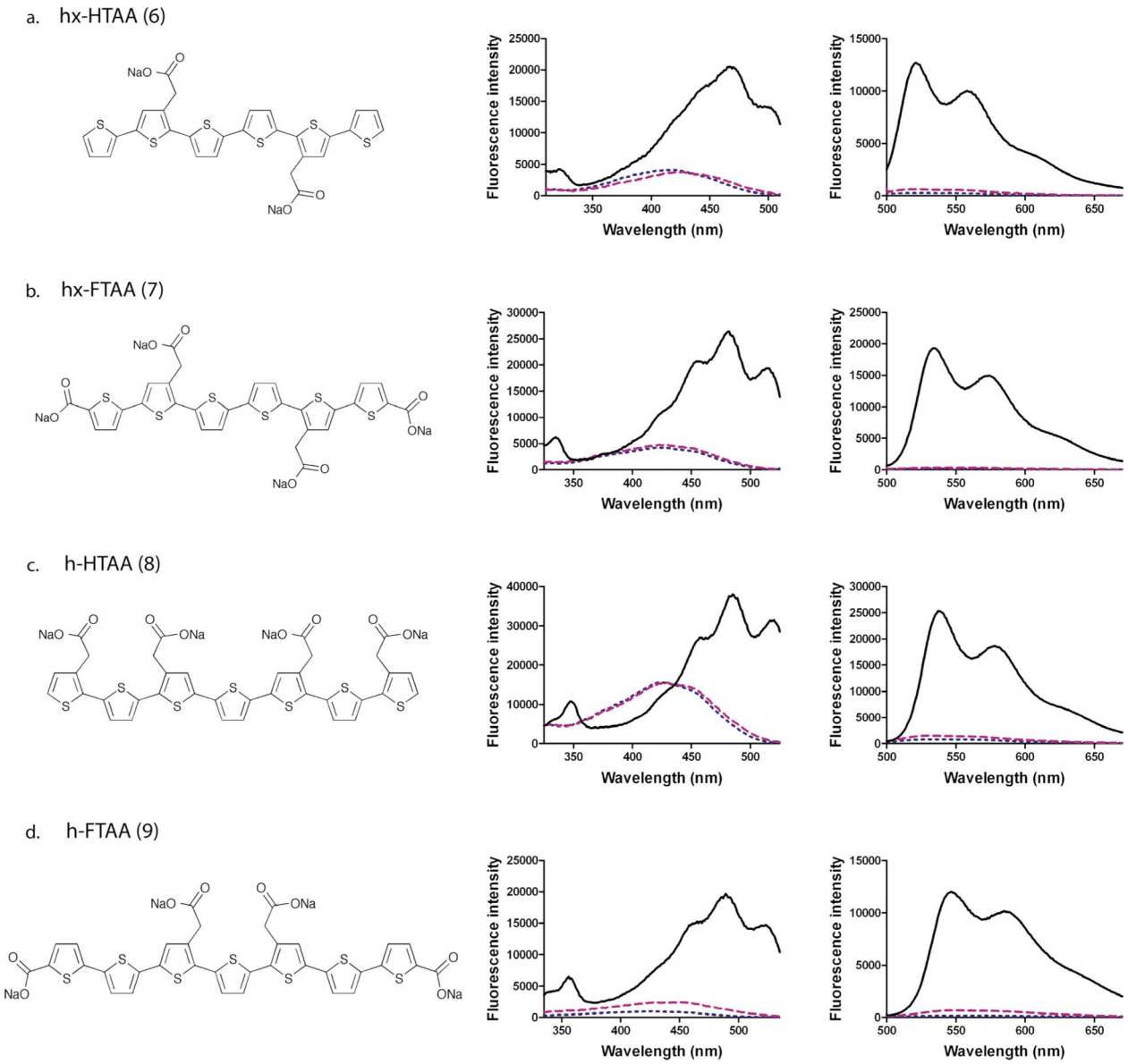

Fig. 2 Chemical structure (left panel), excitation spectrum (middle panel) and emission spectrum (right panel) of hx-HTAA (a), hx-FTAA (b), h-HTAA (c) and h-FTAA (d). The spectral graphs display excitation/emission spectra of the different LCOs in PBS (blue dotted line), in PBS with soluble Aβ1-42 (magenta dashed line) or in PBS with fibrillar Aβ1-42 (black solid line). The excitation/emission wavelengths were 480/522 nm for hx-HTAA, 480/535 nm for hx-FTAA, 480/538 nm for h-HTAA and 480/548 nm for h-FTAA. All probes show well-resolved excitation and emission spectra when binding to Aβ fibrils.

protocol[26] is the lack of agitation during fibrillation and it is well-known that shaking can be used as a parameter to induce rapid formation of amyloid fibrils. Hence, the LCO positive pre-fibrillar species of Aβ1-42 are most likely occurring as a consequence of slowing down the formation of amyloid fibrils as these species could not be observed for p-FTAA when agitation was used during fibrillation.[26]

The kinetic profile monitored by the tetrameric probes t-HTAA, q-HTAA and q-FTAA revealed an onset of fibrillation around 300 min after initiation (Fig. 3a). The kinetic curves were similar to the one obtained with ThT when it came to length of lag phase and fibrillation onset, however, the tetramers reached the plateau phase more rapidly than ThT. The resemblance with ThT was rather expected due to the structural similarity. When the backbone was extended by one thiophene residue, the effect on the detection capacity was obvious. Both p-HTAA and p-FTAA revealed an Aβ1-42 fibrillation process with a growth phase initiated around 60 min, which was 300 min earlier than ThT (Fig. 3b). The pentameric LCOs had reached the plateau phase by the time ThT indicated initiation of growth phase, which further emphasized the difference. Further extension of the thiophene backbone to yield hexamers and heptamers did not significantly enhance nor diminish the effect. hx-HTAA, hx-FTAA, h-HTAA and h-FTAA all bound to Aβ species not detected by ThT with an onset of fibrillation around 90 min (Fig. 3c). hx-FTAA and the two heptamers displayed almost identical kinetic trajectories, whereas

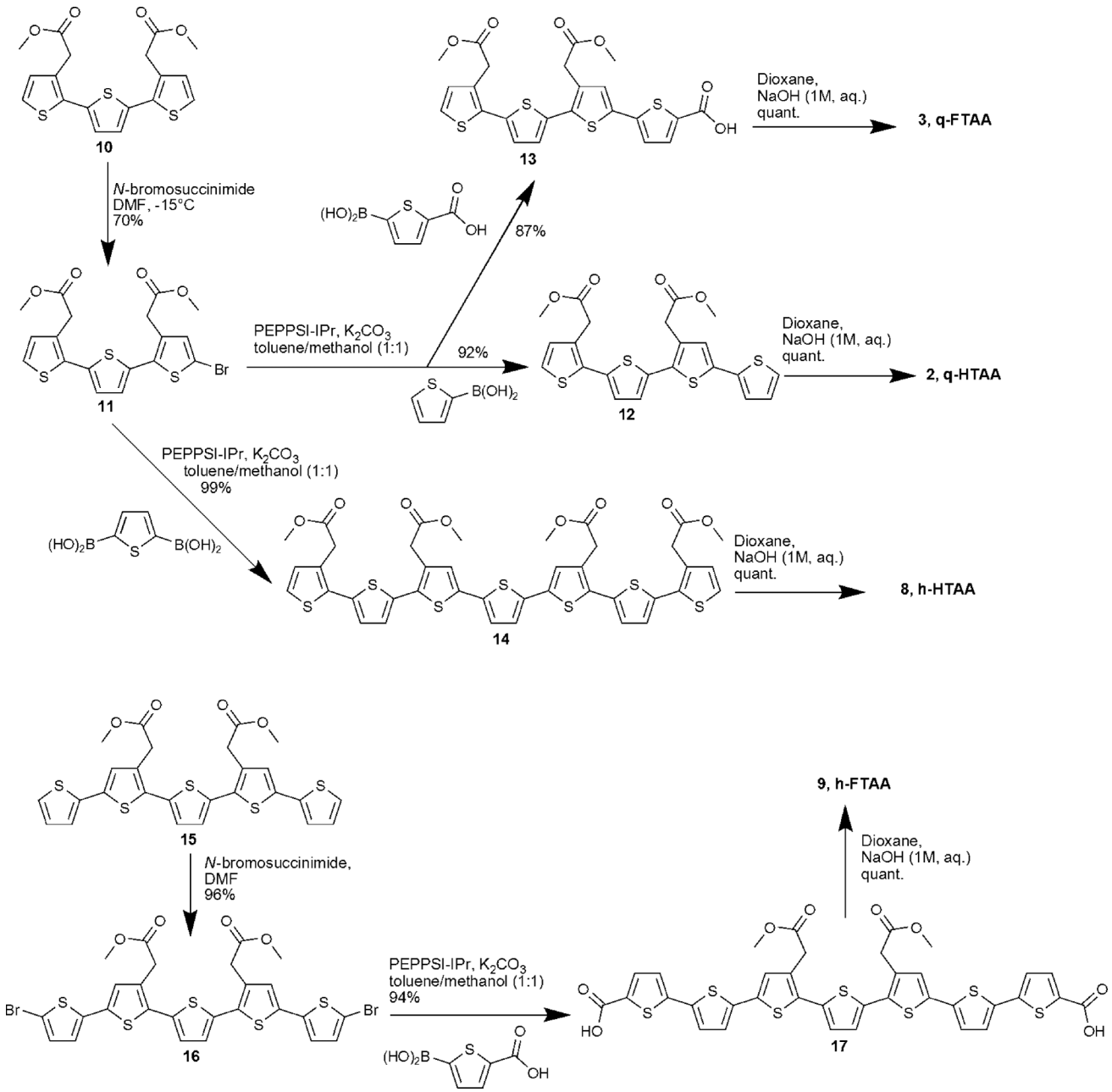

Scheme 1 The synthesis of q-HTAA (**2**), q-FTAA (**3**), h-HTAA (**8**) and h-FTAA (**9**).

hx-HTAA reached the end of the lag phase at a later time-point. Hence, the kinetic results indicated that the length of the backbone, not the chemical substituents, is the crucial factor for the detection of early species preceding the formation of Aβ1-42 fibrils. This finding accentuates the fact that small variations of the LCO structure have a strong impact on their properties for detecting distinct protein assemblies. Hence, having access to a library of different LCOs is highly valuable for assessing a more complete evaluation of different protein aggregation reactions. Since the protocol for monitoring the kinetics of Aβ fibrillation was designed with LCOs present during the reaction (*in situ*), transmission electron microscopy (TEM) was applied to investigate the possible scenario of LCOs enhancing protein aggregation. TEM images were obtained after 180 min of reaction both with and without LCO present and indicated no difference in the fibrillation of Aβ, hence the earlier growth phase monitored by LCOs was not caused by the probes accelerating the kinetics (ESI, Fig. S1†). In addition, kinetic experiments under identical conditions (37 °C, 10 mM phosphate buffer supplemented with 140 mM NaCl and 2.7 mM KCl pH 7.4, quiescent) having only the pentameric, hexameric or heptameric LCOs present or the LCOs mixed with 10 μM bovine serum albumin (BSA) or 100 μM bovine insulin (BI) were also performed. To our knowledge, these proteins will not form protein aggregates under these conditions. All LCOs, except hx-HTAA, showed identical spectra throughout the experiments (1020 min) compared with time-point 0 min, verifying that the characteristic spectroscopic signature obtained from these LCOs during the kinetic measurements of Aβ1-42 fibrillation is associated with

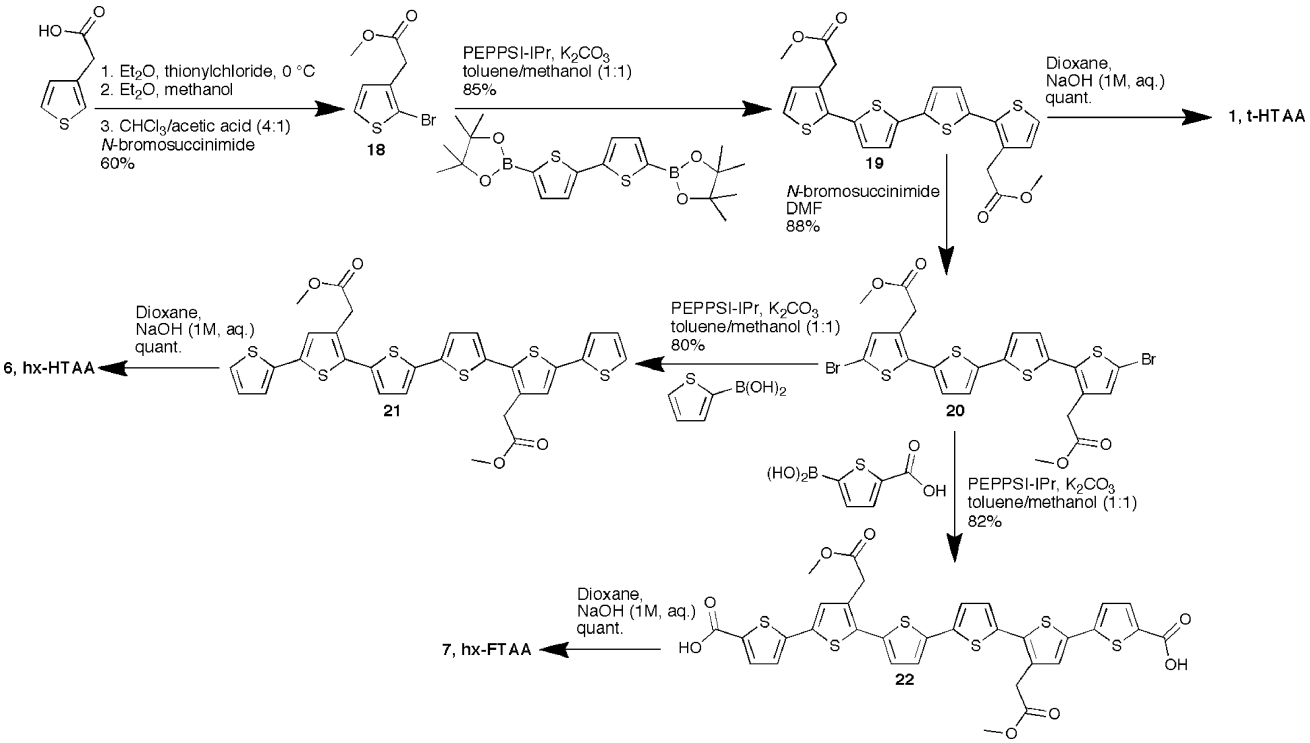

Scheme 2 The synthesis of t-HTAA (**1**), hx-HTAA (**6**) and hx-FTAA (**7**).

pre-fibrillar and fibrillar aggregated species of Aβ1-42 (Fig. S2†). For hx-HTAA we observed a slight decrease of the spectral intensity over time when the dye was free in solution, whereas the opposite occurred when the dye was mixed with BSA (Fig. S2i and S2l†). However, the spectrum was unaffected over the same time period when mixed with BI, and under none of these experiments were we able to obtain a spectroscopic signature similar to the one observed for hx-HTAA interacting with pre-fibrillar and fibrillar aggregated species of Aβ1-42 (Fig. S2j and S2k†). This different behavior from hx-HTAA compared to the other LCOs might occur due to solubility problems of hx-HTAA, as this dye has only two negatively charged side chain functionalities on a hexameric thiophene backbone and hx-HTAA is therefore deemed less suitable for performing kinetic measurements than the other LCOs.

It is well known that the formation of amyloid fibrils is a rather complex event. The simultaneous occurrence of different aggregate species in solution and involvement of heterogeneous aggregation mechanisms render it possible that the LCOs detect the existence of non-fibrillar aggregates occurring in competition with the formation of amyloid fibrils during the Aβ aggregation pathway. Therefore, we utilized the pentameric, hexameric and heptameric LCOs to monitor fibrillation kinetics of BI under acidic conditions, as it was recently shown that insulin under the conditions used assembled into amyloid fibrils through a hexameric oligomer unit.[44] Similar to the results from the Aβ1-42 kinetics, all LCOs detected early non-thioflavinophilic species of insulin and optical density (OD) measurements verified that the LCOs did not affect the fibrillation rate (ESI, Fig. S3 and S4†).

The detection of non-thioflavinophilic Aβ and insulin species by pentameric, hexameric or heptameric LCOs, might be explained by the extended thiophene backbone enhancing the affinity of the LCOs towards these aggregated species. Qin *et al.* recently reported a similar observation for a dimeric version of ThT.[45] However, the mechanism by which ThT and other amyloid ligands recognize fibrillar structures is still poorly understood. In addition to binding, ThT also needs to be sterically locked in order to fluoresce, since free rotation around the benzylamine and benzathiole rings quenches the excited states of ThT.[46–48] Hence, it is possible that ThT and the tetrameric LCOs are capable of binding to the early states seen in the Aβ1-42 and insulin fibrillation, but in their "quenched" mode. Further elongation of the fibrils and more ordered structures might cause the immobilization of the ThT molecule that is necessary for the dramatic increase in fluorescence seen at the later stages of the kinetic experiment. In contrast, the pentameric, hexameric and heptameric LCOs seem to adopt a sterically locked conformation giving rise to a highly fluorescent mode of these LCOs when interacting with protein assemblies preceding the formation of amyloid fibrils. In fact, the plateau phase of pentameric and longer LCOs coincided with the initiation of growth phase monitored by ThT, supporting the theory that ThT needs more ordered fibrils in order to fluoresce. The fluorescence of all investigated LCOs decayed after the plateau phase was reached, which indicated increased stacking of probes due to more densely organised amyloid fibrils. Alternatively different conformations of the LCOs when bound to the early formed assemblies compared to mature fibrillar states could be invoked to explain these observations. However, both the excitation and emission spectral profiles of the LCOs bound to these species are similar, suggesting that the LCOs bind in an analogous fashion to early formed assemblies and mature fibrils. Nevertheless, it is well established that the LCO

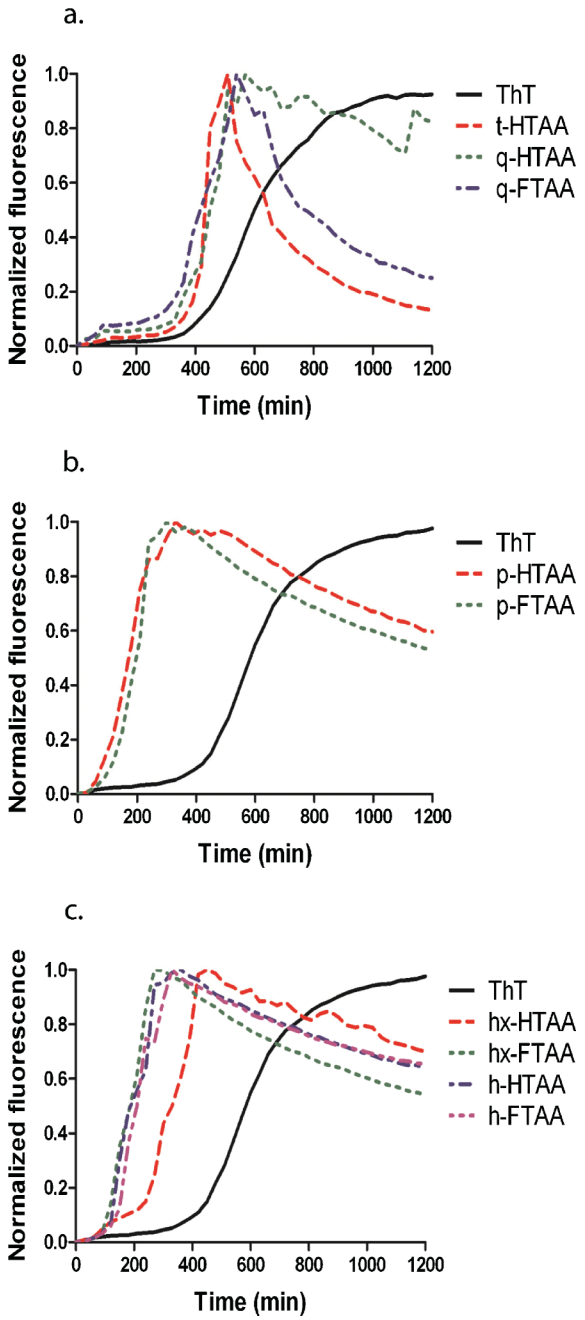

Fig. 3 Fibrillation of recombinant Aβ1-42 monitored by fluorescence from ThT or LCOs. (a) Time plot showing the fibrillation kinetics of Aβ1-42 monitored by fluorescence from ThT (black solid line), t-HTAA (red dashed line), q-HTAA (green dotted line) or q-FTAA (blue dot–dashed line). (b) Time plot of Aβ1-42 fibrillation kinetics monitored by fluorescence from ThT (black solid line), p-HTAA (red dashed line) or p-FTAA (green dotted line). The pentamers detect early non-thioflavinophilic species in the fibrillation pathway and showed initiation of a growth phase already after 60 min. (c) Time plot of Aβ1-42 fibrillation kinetics monitored by fluorescence from ThT (black solid line), hx-HTAA (red dashed line), hx-FTAA (green dotted line), h-HTAA (blue dot-dashed line) or h-FTAA (magenta dot-dot-dashed line). Both hexamers and heptamers detected non-thioflavinophilic species in the fibrillation pathway and showed initiation of the growth phase around 90 min.

p-FTAA fluoresces very strongly when bound to mature amyloid fibrils in tissue (and pelleted fibrils *in vitro*) as observed under the fluorescence microscope.[26,30,32,35] Hence, the decaying intensity effect of LCOs over time seems to occur when LCOs are present *in situ* during fibrillation after the growth of more stable and ordered aggregates in solution/suspension. The full nature of this decrease in intensity will be further elucidated in a future photophysical characterization of all LCOs included in the library.

Obviously, it would be of great interest to determine the nature of the LCO positive non-thioflavinophilic protein assemblies preceding amyloid fibril formation, especially as LCOs and LCPs have proven useful for detection of pathological protein aggregates that go undetected by conventional ligands such as ThT and CR.[23,26,29–34] However, such a study must include extensive fibrillation experiments of Aβ performed under different conditions and also include different variants of the Aβ peptide as it was recently shown that Japanese mutant Aβ rapidly formed amyloid fibrils that were only weakly stained by ThT.[49] So far we can only speculate about the nature of the LCO positive protein assemblies preceding amyloid fibril formation. These assemblies might be fibrillar or non-fibrillar aggregates formed on the Aβ aggregation pathway or in competition with the formation of amyloid fibrils. However, the excitation and emission spectra from the pentameric, hexameric and heptameric LCOs bound to the pre-fibrillar protein assemblies or to mature amyloid fibrils are similar, suggesting that these entities have a related structural arrangement as the LCOs seem to interact in a similar fashion with both of these entities. Initial experiments have also shown that p-FTAA positive Aβ aggregates preceding amyloid fibril formation are more toxic to cells than ThT positive amyloid fibrils (manuscript in progress), suggesting that LCOs would be highly significant as tools for identifying distinct aggregated species occurring during the amyloid fibril formation pathway.

Spectral signatures of LCOs binding to protein aggregates in human AD brain tissue

We have previously reported that p-FTAA can be used to spectrally discriminate between Aβ plaques and NFTs in frozen brain sections from AD patients.[26] Since this spectral ability was believed to depend on the length of the thiophene backbone and the nature of the chemical substituents along the backbone, the library of LCOs displaying variations in these properties was applied to cryosections from human cases with AD pathology. The histological analyses were performed with a fluorescence microscope equipped with a Spectraview system, as this set up offers the possibility to acquire the spectral signatures of each LCO when binding to aggregated Aβ or tau in tissue samples. Additionally, blue (excitation: 405 or 436 nm), green (excitation: 470 or 480 nm) or red (excitation: 535 or 546 nm) long pass filters were utilized to record a complete emission spectral profile of the LCOs. Aβ plaques and NFTs were identified due to their well-known characteristic morphology seen with antibody staining (ESI, Fig. S5†).

All the tetrameric LCOs (t-HTAA, q-HTAA and q-FTAA) specifically stained both Aβ plaques and NFTs in AD affected regions. Moreover, the probes also highlighted cerebrovascular amyloid deposits and dystrophic neurites, two other well-known pathological markers of this disease. All tetramers displayed well-resolved emission spectra upon binding to amyloid deposits, but

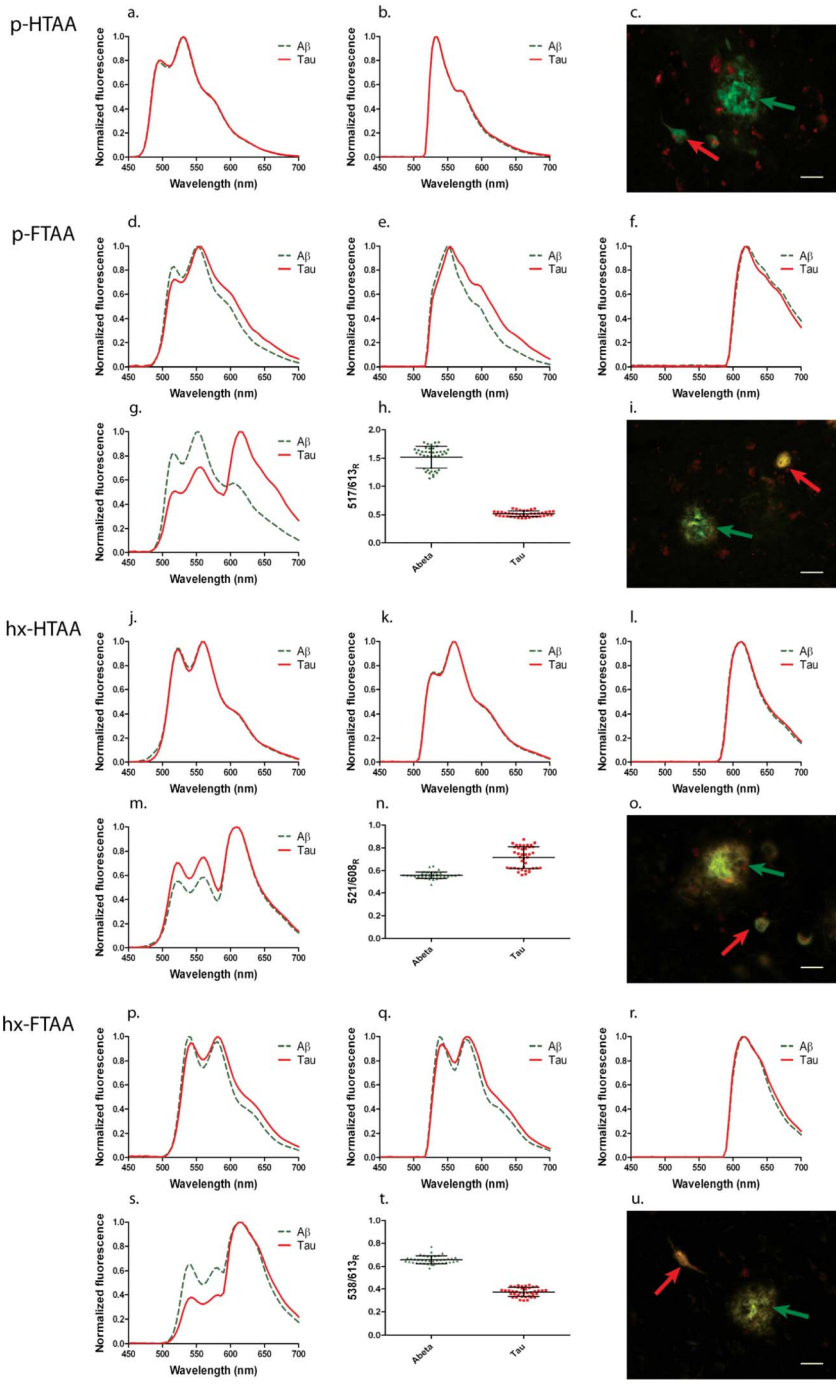

Fig. 4 Emission spectra and fluorescence images of p-HTAA, p-FTAA, hx-HTAA and hx-FTAA bound to pathological hallmarks in AD human brain tissue. (a, d, j, p) The emission spectra of the indicated LCO bound to Aβ plaques (green dashed line) or NFTs (red solid line) when excited at 405 nm. The results show that carboxyl end groups are crucial for obtaining a spectral shift between the two protein entities. (b, e, q) The emission spectra of the indicated LCO bound to Aβ plaques (green dashed line) or NFTs (red solid line) when excited at 470 nm. (f, r) The emission spectra of the indicated LCO bound to Aβ plaques (green dashed line) or NFTs (red solid line) when excited at 546 nm. (k, l) The emission spectra of hx-HTAA bound to Aβ plaques (green dashed line) and NFTs (red solid line) are identical when excited at 480 nm (k) or 535 nm (l). (g, s) The emission spectra of the indicated LCO, bound to Aβ plaques (green solid line) or NFTs (red dashed line), when it has been excited at 405 nm and 546 nm and the resulting emission spectra have been merged together. (m) The resulting emission spectra of hx-HTAA bound to Aβ plaques (green dashed line) and NFTs (red solid line) when the emission at 405 and 535 nm have been merged together. (h, n, t) Plot of the ratio of light intensity emitted at 517 and 613 nm ($517/613_R$) for p-FTAA, 521 and 608 nm ($521/608_R$) for hx-HTAA, 538 and 613 nm ($538/613_R$) for hx-FTAA bound to Aβ plaques (green triangles) or NFTs (red squares) shown with standard deviation. The intensities are obtained from the double excitation spectra. (c, i, o, u) Fluorescence images of human AD brain sections stained with the indicated LCO. The images visualize typical pathological entities, Aβ plaques (green arrow) or NFTs (red arrow), from which the emission spectra were obtained. Scale bars represent 20 μm.

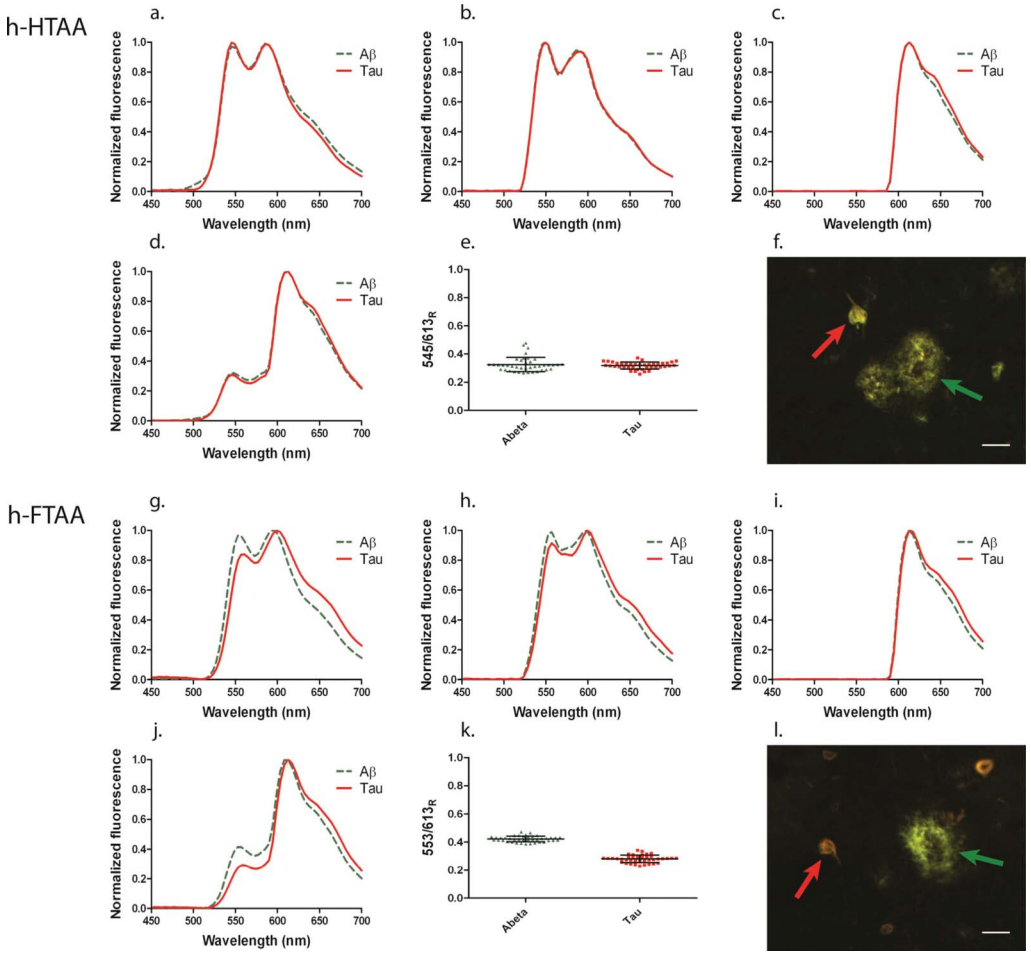

Fig. 5 Emission spectra and fluorescence images of h-HTAA and h-FTAA bound to pathological hallmarks in AD human brain tissue. (a, g) The resulting emission spectra of the indicated LCO bound to Aβ plaques (green dashed line) and NFTs (red solid line) excited at 405 nm. (b, h) The emission spectra of the indicated LCO bound to Aβ-plaques (green dashed line) and NFTs (red solid line) when excited at 470 nm. (c, i) The emission spectra of the indicated LCO bound to Aβ plaques (green dashed line) and NFTs (red solid line) when excited at 546 nm. (d, j) The resulting emission spectra of the indicated LCO bound to Aβ plaques (green dashed line) and NFTs (red solid line) when the emission at 405 and 546 nm have been merged together. (e, k) Plots of the ratio of light intensity emitted at 545 nm and 613 nm ($545/613_R$) for h-HTAA or 553 nm and 613 nm ($553/613_R$) for h-FTAA when bound to Aβ plaques (green triangles) or NFTs (red squares) shown with standard deviation. The intensities are obtained from the double excitation spectra. (f, l) Fluorescence images of human AD brain sections stained with the indicated LCO. The images visualize typical pathological entities, Aβ plaques (green arrow) or NFTs (red arrow), from which the emission spectra were obtained. Scale bars represent 20 μm.

there was no significant spectral distinction between Aβ and tau deposits when using two different long pass filters (excitation at 405 or 436 nm) (ESI, Fig. S6†). The tetrameric LCOs showed no significant emission when using a long pass filter for longer wavelengths (excitation: 535 or 546 nm). It also became evident that the tetrameric probes tended to photobleach, which was indicated by the change of the normally blue-shifted emission spectra against longer wavelengths upon prolonged exposure to light.

In accordance with previous results,[26] LCOs having a pentameric thiophene backbone (p-HTAA and p-FTAA) displayed selective binding towards protein aggregates and these pathological hallmarks were also specifically stained by LCOs having a hexameric (hx-HTAA and hx-FTAA) (Fig. 4) or a heptameric thiophene backbone (h-HTAA and h-FTAA) (Fig. 5). Similar to the tetrameric LCOs, all longer LCOs showed well-resolved emission spectra upon binding to Aβ or tau deposits using blue (excitation: 405 nm) or green (excitation: 470 or 480 nm) long pass filters. Secondly, these LCOs also exhibited a substantial amount of emission at longer wavelengths when a red long pass filter was used (excitation: 535 or 546 nm) (Fig. 4 and Fig. 5). A red-shift of the emission maxima was observed as the electronic conjugation length of the thiophene backbone was extended and the "F" variants always showed more reddish spectra compared to their "H" counterparts, mainly due to extension of the conjugated thiophene backbone by carboxyl groups. Interestingly, the difference in spectral shift was most pronounced when comparing p-FTAA with p-HTAA, indicating that the maximum effect of the carboxyl moieties on the electronic system is obtained with a pentameric thiophene backbone.

When examining the spectral differences for Aβ plaques and NFTs, the pentameric, hexameric and heptameric "F" variants showed a clear difference in the overall appearance of the emission spectra (excitation: 405, 470 or 480 nm) for these pathological hallmarks, whereas this spectral difference was not observed for the "H" counterparts (Fig. 4 and Fig. 5). Binding of the "F"

variants to aggregated tau in NFTs and dystrophic neurites displayed increased contribution of red-shifted wavelengths compared to the spectra from Aβ plaques. This was evident from the disappearance of the most blue shifted peak and a more pronounced shoulder at longer wavelengths (Fig. 4 and Fig. 5). By exciting the LCOs at 405 nm and 535/546 nm and then merging the resulting emission spectra, the spectral difference became even more evident, since this operation highlights both green and red contributions to the spectrum. When plotting the ratio of the intensity of the emitted light at the blue-shifted and red-shifted emission maxima (Fig. 4 and Fig. 5), there was a clear separation between Aβ and tau aggregates proving the discrepancy in emission from the "F" variants upon binding to the respective pathological entity. The merged emission spectrum of one of the "H" variants, hx-HTAA, also revealed a distinction in color between the protein aggregates. The spectra from tau deposits were green-shifted compared to the spectra observed from Aβ plaques, a result that was opposite that of the "F" variants. The ratio plot showed a rather wide distribution of the tau aggregates and a partial overlap between the two pathological hallmarks (Fig. 4n).

When the ratio plots were compared, it became evident that the "F" variants were superior LCOs for spectral distinction of the two pathological hallmarks seen in AD. Secondly, p-FTAA surpassed both hx-FTAA and h-FTAA, again showing that the maximum effect of the carboxyl extensions on the electronic system was obtained having a pentameric thiophene backbone. Although it is evident that the carboxyl groups are crucial to obtain a spectral difference between Aβ and tau deposits, the spectral observations cannot explain the difference between these two protein aggregates on a molecular basis. The variation of spectral fingerprints reported for LCPs bound to distinct protein aggregates, such as prion strains or heterogenic populations of Aβ deposits, has mainly been interpreted as a result of a conformational variety of the protein aggregates, leading to separation and stacking of polythiophene chains.[22,23] However, the distinct spectral signatures from the LCOs reported herein were different, as the spectral distinction between Aβ and tau deposits was dependent on an extension of the thiophene backbone with carboxyl groups rather than on a conformational change of the thiophene backbone. The fact that the polymeric LCP PTAA was incapable of spectrally discriminating Aβ and tau deposits in human tissue[26] also indicates that the underlying molecular mechanism of the spectral signature from p-FTAA, hx-FTAA and h-FTAA might not be dependent on conformational differences between Aβ and tau deposits. Instead, the red-shift in emission might arise from interplay between the end carboxyl groups extending the LCO backbone and chemical groups in the binding pocket of tau aggregates. Tau aggregates are known to carry a diverse array of chemical modifications,[50] including extensive phosphorylations, and these modifications might affect the conjugation system causing the observed red-shift of the emission.

Conclusions

In conclusion, we have shown that certain molecular requirements are necessary for achieving an anionic oligothiophene-based ligand capable of detecting non-thioflavinophilic aggregated species preceding amyloid fibril formation and for obtaining distinct spectral signatures of the two main pathological hallmarks observed in AD. Preferably, such a ligand should have a backbone consisting of five to seven thiophene units and carboxyl groups extending the conjugated thiophene backbone. The addition of such LCOs to the toolkit of fluorescent ligands will be important for studying the underlying molecular events of protein aggregation diseases and for obtaining sensitive diagnostic tools for these diseases.

Experimental

General methods

Organic extracts were dried over anhydrous magnesium sulfate, filtered and concentrated *in vacuo* at 40 °C. 3-Thiopheneacetic acid, 2-thiopheneboronic acid and PEPPSI-IPr ([1,3-bis(2,6-diisopropylphenyl)imidazol-2-ylidene](3-chloropyridyl)palladium(II) dichloride) are commercially available from Sigma-Aldrich Co (Sigma-Aldrich, St. Louis, MO, USA). 5-(Dihydroxyboryl)-2-thiophenecarboxylic acid was acquired from Maybridge (Maybridge, Cambridge, UK). UV/VIS absorbance spectra were recorded with a Tecan Saphire² microplate reader (Tecan, Männedorf, Switzerland) or a Hitachi U-1900 spectrophotometer (Hitachi, Tokyo, Japan). FT-IR spectra were recorded using a Perkin Elmer Spectrum 1000 spectrometer (Perkin Elmer, Waltham, MA, USA). NMR spectra were recorded on a Varian instrument (^{1}H 300 MHz, ^{13}C 75.4 MHz, Varian Inc., Santa Clara, CA, USA). Chemical shifts were assigned with the solvent residual peak as a reference according to Gottlieb *et al.*[51] Thin layer chromatography (TLC) was carried out on Merck precoated 60 F254 plates (Merck, Whitehouse Station, NJ, USA) using UV light (λ = 254 nm and 366 nm) and charring with ethanol/sulfuric acid/*p*-anisaldehyde/acetic acid 90 : 3 : 2 : 1 for visualization. Flash column chromatography (FC) was performed using silica gel 60 (0.040–0.063 mm, Merck). Gradient HPLC-MS was performed on a Gilson system (Gilson, Middleton, WY, USA). Column: Waters X-Bridge C-18 5 µ, 250 × 15 mm and Waters X-Bridge C-18 2.5 µ, 150 × 4.6 mm for semipreparative and analytical runs respectively; using acetonitrile with 0.05% formic acid and deionized water with 0.05% formic acid as mobile phase. For preparative reversed phase purifications a VersaFlash™ (Sigma–Aldrich) system equipped with VersaPak™ C18 cartridges was used. MALDI-TOF MS was recorded in linear positive mode with the analyte as matrix. Normal work up means that the organic extracts were dried on $MgSO_4$, filtered and concentrated *in vacuo*.

General procedure A: Suzuki coupling with a thiopheneboronic acid and a mono- or dibrominated oligothiophene

To a solution of the brominated oligothiophene (1 mmol) in toluene/methanol (1 : 1, 5 mL, degassed) K_2CO_3 (3 equiv./bromine), the desired thiopheneboronic acid (2 equiv./bromine) and PEPPS-IPr (0.02 equiv.) were added. The mixture was heated to 70 °C for 15 min, whereupon work-up followed.

General procedure B: dibromination of an oligothiophene

To a solution of the oligothiophene (1 mmol) in DMF (5 mL, −15 °C) NBS (2 mmol) was added slowly, whereupon the reaction reached room temperature. After 2 h, the reaction was diluted with toluene, washed with HCl (1 M, aq.) twice and brine three times.

General procedure C: Suzuki coupling with a diboronic acid or ester with a monobrominated oligothiophene.

The desired boronic derivative (1 mmol), the monobrominated oligothiophene (3 mmol), K_2CO_3 (4 mmol) and PEPPSI-IPr (0.02 mmol) were dissolved in degassed toluene/methanol (1 : 1, 5 mL) and heated to 70 °C for 15 min, whereupon work-up followed.

General procedure D: hydrolysis methylesters

To a solution of the oligothiophene (1 mmol) in dioxane (10 mL), NaOH (1 M, 1.5 equiv./acid and ester) was added. When precipitation started, H_2O (10 mL) was added. When only product was seen on MS, the reaction was lyophilized and stored under refrigerated, dark conditions.

Synthesis of t-HTAA (1)

General procedure D was applied to compound **19** to give the product t-HTAA (**1**) quantitatively. UV Abs: λ_{max} (dH_2O)/nm 385. FT-IR ν_{max} (KBr pellet): 638, 690, 786, 833, 1284, 1387, 1560, 1650, 3484 cm^{-1}.

^{1}H NMR (D_2O) δ: 3.49 (s, 4H), 6.78 (d, J = 3.7 Hz, 2H), 6.83 (d, J = 4.9 Hz, 2H), 6.87 (d, J = 3.7 Hz, 2H), 7.12 (d, J = 4.9 Hz, 2H).

^{13}C NMR (D_2O) δ: 38.2, 124.4, 124.6, 126.7, 131.7, 132.0, 133.8, 134.9, 136.4, 178.0.

Synthesis of q-HTAA (2)

General procedure D was applied to compound **12** to give the product q-HTAA (**2**) quantitatively. UV Abs: λ_{max} (dH_2O)/nm 370. FT-IR ν_{max} (KBr pellet): 641, 691, 835, 1235, 1268, 1384, 1420, 1498, 1566, 3059, 3395 cm^{-1}.

^{1}H NMR (D_2O) δ: 3.63 (s, 2H), 3.69 (s, 2H), 7.01 (dd, J = 5.0, 3.6 Hz, 1H), 7.05 (d, J = 5.2 Hz, 1H), 7.08 (s, 3H), 7.16 (dd, J = 3.6, 1.1 Hz, 1H), 7.32 (dd, J = 5.0, 1.1 Hz, 1H), 7.36 (d, J = 5.2 Hz, 1H).

^{13}C NMR (D_2O) δ: 38.1, 124.1, 124.7, 125.2, 126.6, 128.0, 128.4, 130.8, 131.5, 131.8, 134.0, 134.6, 135.0, 135.4, 135.7, 136.7, 179.5, 180.0.

Synthesis of q-FTAA (3)

General procedure D was applied to compound **13** to give the product q-FTAA (**3**) quantitatively. UV Abs: λ_{max} (dH_2O)/nm 392. FT-IR ν_{max} (KBr pellet): 636, 688, 775, 788, 866, 1394, 1448, 1568, 3416 cm^{-1}.

^{1}H NMR (D_2O): δ 3.68 (s, 4H), 7.01 (d, J = 5.1 Hz, 1H), 7.15 (d, J = 3.9 Hz, 1H), 7.20 (d, J = 3.9 Hz, 1H), 7.23 (d, J = 3.9 Hz, 1H), 7.23 (s, 1H), 7.36 (d, J = 5.1 Hz, 1H), 7.46 (d, J = 3.9 Hz, 1H).

^{13}C NMR (D_2O): δ 38.3, 124.3, 124.5, 126.3, 126.6, 129.1, 131.7, 131.9, 132.0, 132.1, 133.8, 134.2, 134.4, 135.1, 136.0, 139.5, 141.0, 169.8, 179.5, 180.0.

Synthesis of hx-HTAA (6)

General procedure D was applied to compound **21** to give the product hx-HTAA (**6**) in quantitative yield. UV Abs: λ_{max} (dH_2O)/nm 418. FT-IR ν_{max} (KBr pellet): 649, 687, 786, 866, 1384, 1411, 1456, 1576, 3422 cm^{-1}.

^{1}H NMR (DMSO-d_6) δ: 3.76 (s, 4H); 7.11 (dd, J = 3.6, 5.2 Hz, 2H); 7.24 (d, J = 3.9 Hz, 2H); 7.27 (s, 2H); 7.34 (dd, J = 1.1, 3.6 Hz, 2H); 7.39 (d, J = 3.9 Hz, 2H); 7.55 (dd, J = 1.1, 5.2 Hz, 2H).

^{13}C NMR (DMSO-d_6) δ: 35.4, 125.2, 126.1, 126.7, 128.1, 128.7, 129.2, 130.9, 133.5, 134.3, 135.3, 136.3, 136.6, 172.3.

Synthesis of hx-FTAA (7)

General procedure A was applied to **20** and 5-(dihydroxyboryl)-2-thiophenecarboxylic acid. After the reaction, the mixture was acidified with acetic acid, diluted with ethyl acetate and washed three times with H_2O and subjected to normal work-up. The crude product was recrystallized from dioxane to give **22** (82%) as a red powder. General procedure D was applied to **22** to afford the product hx-FTAA (**7**) quantitatively as a red salt. UV Abs: λ_{max} (dH_2O)/nm 428. FT-IR ν_{max} (KBr pellet): 722, 783, 803, 1384, 1443, 1462, 1570, 1630, 3432 cm^{-1}.

^{1}H NMR (D_2O) δ: 3.68 (s, 4H); 7.00 (d, J = 4.0 Hz, 2H), 7.02 (d, J = 4.0 Hz, 2H), 7.04 (s, 2H), 7.09 (d, J = 3.9 Hz, 2H), 7.38 (d, J = 3,9 Hz, 2H).

^{13}C NMR (D_2O) δ: 38.6, 124.2, 124.6, 126.4, 129.3, 131.9, 132.3, 133.9, 134.2, 134.6, 136.4, 139.3, 140.9, 169.8, 179.3.

Synthesis of h-HTAA (8)

General procedure C was applied to **11** and thiophene-2,5-diboronoic acid. After the reaction, the solution was decanted and evaporated to relative dryness. The remaining portion in the reaction vessel, containing salts, was repeatedly washed with EtOAc (5 × 20 mL) and combined with the mother liquor, which was then washed with water (2 × 50 mL), then 1 M HCl solution (2 × 50 mL). The organic phase was dried over $MgSO_4$, filtered and evaporated to dryness. The solid was slurried in ethanol, filtered and dried under vacuum giving the compound **14** (99%) as an amorphous orange/red powder. General procedure D was applied to **14** to afford the product h-HTAA (**8**) quantitatively as a red salt. UV Abs: λ_{max} (dH_2O)/nm 432. FT-IR ν_{max} (KBr pellet): 630, 705, 788, 834, 916, 1221, 1253, 1411, 1700, 2921, 3432 cm^{-1}.

^{1}H NMR (D_2O) δ: 7.07 (d, J = 5.1 Hz, 2H); 6.84 (s, 2H); 6.81 (d, J = 5.2 Hz, 2H); 6.70 (m, 4H), 6.49 (s, 1H); 4.65 (s, 8H).

^{13}C NMR (D_2O) δ: 38.4, 38.5, 124.4, 124.9, 126.3, 126.4, 128.3, 131.3, 131.5, 132.1, 133.5, 134.2, 135.3, 135.5, 135.7, 179.3, 179.9.

Synthesis of h-FTAA (9)

General procedure A was used with 5-(dihydroxyboryl)-2-thiophenecarboxylic acid and **16**. After the reaction was finished, the solution was decanted and evaporated to relative dryness. The remaining portion in the reaction vessel, containing salts, was repeatedly washed with EtOAc (5 × 20 mL) and combined with the mother liquor, which was then washed with water (2 × 50 mL), then 1 M HCl solution (2 × 50 mL). The organic phase was dried over $MgSO_4$, filtered and evaporated to dryness. The solid was slurried in ethanol, filtered and dried under vacuum giving **17** in 94% yield as an amorphous orange/red powder. General procedure D was applied to **17** to afford the product h-FTAA (**9**) quantitatively as a red salt. UV Abs: λ_{max} (dH_2O)/nm 433. FT-IR ν_{max} (KBr pellet): 774, 1383, 1443, 1464, 1521, 1569, 3406 cm^{-1}.

^{1}H NMR (D_2O) δ: 3.6 (bs, 4H), 6.6–6.8 (bm, 10H), 7.3 (d, J = 3.7 Hz).

^{13}C NMR (D2O) δ: 38.8, 124.1, 125.0, 125.8, 128.4, 131.7, 131.9, 133.9, 134.0, 135.2, 136.3, 139.4, 141.0, 169.7, 179.1.

Synthesis of product 11

NBS (2.35 g, 13.2 mmol) was added to solution of **10** (5.36 g, 13.7 mmol) dissolved in DMF (100 mL) at −15 °C, after which the stirring solution was allowed to achieve room temperature and stir for a further hour. When TLC and MALDI-TOF MS indicated that the reaction was complete the mixture was diluted with toluene and washed with brine and water before being subjected to normal work-up. The product was purified on reversed phase (acetonitrile/water (30 : 70 0.05% formic acid)) to afford compound **11** (70%). UV Abs: λ_{max} (ACN)/nm 340. FT-IR ν_{max} (KBr pellet): 626, 711, 764, 792, 833, 989, 1137, 1179, 1203, 1225, 1251, 1328, 1417,1434, 1732, 3446 cm^{-1}.

^{1}H NMR ($CDCl_3$) δ: 3.67 (s, 4H), 3.73 (s, 6H), 6.99 (s, 1H), 6.99 (d, J = 5.6 Hz, 1H), 7.06 (d, J = 3.5 Hz, 1H), 7.10 (d, J = 3.5 Hz, 1H), 7.19 (d, J = 5.6 Hz, 1H)

^{13}C NMR ($CDCl_3$) δ: 34.1, 34.4, 51.9, 52.0, 111.2, 124.7, 127.1, 127.6, 130.3, 130.4, 130.8, 132.3. 132.8, 133.9, 134.2, 136.1, 170.6, 171.0.

Synthesis of product 12

General procedure A was used with **11** and 2-thiopheneboronic acid. After the reaction, the product was purified by FC (toluene) to afford compound **12** (92%) as a yellow powder. UV Abs: λ_{max} (ACN)/nm 368. FT-IR ν_{max} (KBr pellet): 630, 702, 832, 1014, 1171, 1197, 1251, 1333, 1434, 1734, 2949, 3102, 3438 cm^{-1}.

^{1}H NMR ($CDCl_3$) δ: 3.74 (s, 3H), 3.75 (s, 3H), 3.78 (s, 2H), 3.80 (s, 2H), 7.02 (dd, J = 5.1, 3.6 Hz, 1H), 7.06 (d, J = 5.3 Hz, 1H), 7.13 (s, 1H), 7.15 (d, J = 3.7 Hz, 1H), 7.18 (d, J = 3.7 Hz, 1H), 7.18 (dd, J = 3.6, 1.1 Hz, 1H), 7.23 (dd, J = 5.1, 1.1 Hz, 1H), 7.26 (d, J = 5.3 Hz, 1H).

^{13}C NMR ($CDCl_3$) δ: 34.8, 34.9, 52.3, 52.4, 124.2, 124.9, 125.0, 126.9, 127.4, 127.5, 128.0, 130.5, 130.6, 131.0, 131.8, 132.9, 135.5, 135.9, 136.3, 136.8, 171.2, 171.4.

Synthesis of 13

General procedure A was used with **11** and 5-(dihydroxyboryl)-2-thiophenecarboxylic acid. After the reaction, acetic acid and ethyl acetate were added to the reaction mixture. The solution was washed three times with H_2O and recrystallized from methanol to afford compound **13** (87%) as a red powder. UV Abs: λ_{max} (ACN)/nm 378. FT-IR ν_{max} (KBr pellet): 748, 784, 803, 852, 896, 935, 972, 1013, 1044, 1108, 1176, 1203, 1299, 1455, 1506, 1532, 1668, 1733, 2516, 2951, 3444 cm^{-1}.

^{1}H NMR (DMSO-d_6) δ: 3.65 (s, 3H), 3.67 (s, 3H), 3.84 (s, 2H), 3.88 (s, 3H), 7.10 (d, J = 5.1 Hz, 1H), 7.25 (d, J = 3.9 Hz, 1H), 7.30 (d, J = 3.9 Hz, 1H), 7.39 (d, J = 3.9 Hz, 1H), 7.46 (s, 1H), 7.56 (d, J = 5.1 Hz, 1H), 7.68 (d, J = 3.9 Hz, 1H).

^{13}C-NMR (DMSO-d_6) δ: 34.0, 34.1, 51.9, 52.0, 125.0, 125.5, 127.3, 127.7, 129.6, 131.2, 131.3, 131.4, 132.1, 132.3, 133.3, 133.5, 133.9, 134.2, 135.5, 141.6, 162.5, 170.4, 170.7.

Synthesis of product 16

General procedure B was applied to compound **15**. The crude product was purified on flash silica gel chromatography (heptane/ethyl acetate 7 : 3) followed by purification of the desired fractions by reversed phase chromatography (CH_3CN/H_2O gradient 60 : 40 → 80 : 20 → 100 : 0). The isolated fractions were combined and dried under reduced pressure giving compound **16** (96%) as an amorphous orange/red powder. UV Abs: λ_{max} (ACN)/nm 389. FT-IR ν_{max} (KBr pellet): 792, 840, 965, 1013, 1172, 1197, 1254, 1336, 1428,1500, 1733, 2950, 3437 cm^{-1}.

^{1}H NMR (DMSO-d_6) δ: 3.66 (s, 6H); 3.85 (s, 4H); 7.19 (d, J = 3.9 Hz, 2H); 7.24 (d, J = 3.9 Hz, 2H); 7.27 (d, J = 0.8 Hz, 4H).

^{13}C NMR (DMSO-d_6) δ: 169.9; 137.0; 134.2; 133.4; 131.8; 131.4; 130.7; 127.9; 127.3; 124.8; 110.4; 51.5; 33.8.

Synthesis of product 18

3-Thiopheneacetic acid (14.2 g, 100 mmol) was dissolved in diethyl ether (150 mL, dry) and cooled to 0 °C. Thionyl chloride (15.8 mL, 300 mmol) was added slowly. After 1 h, the solution was evaporated, dissolved in diethyl ether (150 mL, dry) and cooled in an ice bath. Methanol (dry, excess) was added slowly to the solution and allowed to stir at room temperature for 1 h. The solvents were evaporated while the product was redissolved in ethyl acetate and washed with $NaHCO_3$ (sat. aq.) followed by water. The methyl ester of 3-thiopheneacetic acid was dissolved in chloroform/acetic acid (4 : 1, 180 mL) and NBS (17.8 g, 100 mmol) was added portionwise over two hours. After 18 h the solution was washed with $NHCO_3$ (sat., aq.) until basic. FC (heptane/ethyl acetate 9 : 1) gave compound **18** (60%) as a colorless oil. UV Abs: λ_{max} (ACN)/nm 236, 194. FT-IR ν_{max} (KBr discs): 604, 636, 682, 701, 828, 893, 911, 971, 995, 1014, 1094, 1167, 1198, 1265, 1334, 1375, 1413, 1435, 1541, 1738, 2841, 2951, 2999, 3108, 3460 cm^{-1}.

^{1}H NMR (D_2O) δ: 3.63 (s, 2H); 3.71 (s, 3H); 6.92 (d, J = 5.5 Hz, 1H); 7.23 (d, J = 5.5 Hz, 1H).

^{13}C NMR (D_2O) δ: 34.9, 52.2, 111.7, 125.9, 128.8, 133.6, 170.6.

Synthesis of product 19

General procedure C was used with **18** and 2,2′-bithiophene-5,5′-diboronic acid bis(pinacol) ester. After the reaction the solution was diluted with toluene and washed with HCl (1 M, aq.) twice and brine 3 three times. The product was purified by FC (toluene) to give compound **19** (85%) as yellow oil. R_f: 0.42 (toluene/ethyl acetate 18 : 1). UV Abs: λ_{max} (ACN)/nm 371. FT-IR ν_{max} (KBr pellet): 638, 686, 716, 798, 835, 868, 925, 963, 1018, 1058, 1079, 1123, 1215, 1265, 1300, 1426, 1437, 1453, 1736, 2953, 3448 cm^{-1}.

^{1}H NMR ($CDCl_3$) δ: 3.74 (s, 6H); 3.80 (s, 4H), 7.06 (d, J = 5.2 Hz, 2H); 7.10 (d, J = 3.77 Hz, 2H); 7.23 (d, J = 3.77 Hz, 2H); 7.25 (d, J = 5.2 Hz, 2H).

^{13}C NMR ($CDCl_3$) δ: 34.7, 52.3, 124.4, 124.7, 127.6, 130.4, 130.5, 133.1, 134.3, 137.5, 171.4.

Synthesis of product 20

General procedure B was used on **19**. The crude product was purified by FC (toluene) to give compound **20** (88%). UV Abs: λ_{max} (ACN)/nm 375. UV Abs: λ_{max} (ACN)/nm 375. FT-IR ν_{max}

(KBr pellet): 625, 791, 830, 1002, 1131, 1195, 1217, 1285, 1304, 1334, 1425, 1455, 1505, 1734, 2954, 3439 cm^{-1}.

^1H NMR ($CDCl_3$) δ: 3.72 (s, 4H); 3.74 (s, 6H); 7.03 (s, 2H); 7.05 (d, J = 3.77 Hz, 2H); 7.30 (d, J = 3.77 Hz, 2H).

^{13}C NMR ($CDCl_3$) δ: 34.6, 52.5, 111.7, 124.7, 128.2, 131.2, 133.2, 133.1, 137.9, 170.9.

Synthesis of product 21

General procedure A was used with 2-thiopheneboronic acid and **20**. After the reaction was finished, chloroform was added and the solution was washed with HCl (1 M, aq.) twice and brine three times. The crude product was recrystallized from toluene to give compound **21** (80%) as red crystals. UV Abs: λ_{max} (ACN)/nm 402. FT-IR ν_{max} (KBr pellet): 686, 814, 842, 1020, 1139, 1229, 1272, 1308, 1433, 1507, 1725, 2948, 3428 cm^{-1}.

^1H NMR ($CDCl_3$) δ: 3.76 (s, 6H); 3.79 (s, 4H); 7.03 (dd, J = 3.63, 5.10 Hz, 2H); 7.13 (s, 2H); 7.13 (d, J = 3.79 Hz, 2H); 7.16 (d, J = 3.79 Hz, 2H); 7.19 (dd, J = 1.15, 3.61 Hz, 2H); 7.24 (dd, J = 1.15, 5.10 Hz, 2H).

^{13}C NMR ($CDCl_3$) δ: 35.0, 52.4, 124.2, 124.7, 125.0, 126.9, 127.6, 128.0, 131.1, 131.9, 134.2, 136.3, 136.8, 137.5 171.2.

Detection of pre-fibrillar and fibrillar Aβ and insulin species

Recombinant Aβ1-42 (rPeptide, Athens, GA, USA, lyophilized from hexafluoroisopropanol and dissolved in 2 mM NaOH) was diluted in 10 mM phosphate buffer supplemented with 140 mM NaCl and 2.7 mM KCl (PBS pH 7.4) to a final concentration of 10 μM and added to a 96-well microtiter plate (Corning Incorporated, Corning, NY, USA). Stock solutions of LCOs (1.5 mM) and ThT (2 mM) were diluted in distilled water to 15 μM and added to the wells to a final concentration of 0.3 μM. The samples were incubated at 37 °C in a Tecan Saphire² microplate reader (Tecan, Männerdorf, Switzerland) and the emission spectrum of each probe was collected every 30 min. The emission spectra for t-HTAA, q-HTAA and q-FTAA were collected between 470–640 nm with excitation wavelength 430 nm. The emission spectra for p-HTAA and p-FTAA were collected between 480–650 nm with excitation wavelength 450 nm. The emission spectra for hx-HTAA, hx-FTAA, h-HTAA and h-FTAA were collected between 500–670 nm with excitation wavelength 480 nm. ThT was excited at 430 nm (emission between 470–640 nm) when used as a reference for the tetramers and it was excited at 450 nm (emission between 480–650 nm) when used as a reference for the pentamers, hexamers and heptamers. All samples were done in triplicate. Experiments replacing the Aβ1-42 peptide with 10 μM bovine serum albumin (MP Biomedicals, Solon, USA) or 100 μM bovine insulin (I6634, Sigma Aldrich) were also performed in a similar fashion.

Excitation spectra for the LCOs were obtained at time-point 0 min (right after the addition of soluble Aβ1-42) and for probes binding to Aβ1-42 fibrils (at the plateau phase). The excitation spectra for t-HTAA (emission at 490 nm), q-HTAA (emission at 490 nm), q-FTAA (emission at 505 nm) and p-HTAA (emission at 490 nm) were collected between 270–470 nm. The excitation spectra for p-FTAA (emission at 507 nm), hx-HTAA (emission at 522 nm), hx-FTAA (emission at 535 nm), h-HTAA (emission at 538 nm) and h-FTAA (emission at 548 nm) were collected between 300–500, 310–510, 325–525, 335–535 nm, respectively.

Emission spectrum and excitation spectrum for each probe in PBS were also obtained using the same settings as described above.

Amyloid fibrils of bovine insulin were prepared according to a previously reported protocol.[35,44] In brief, a stock solution containing 5 mg mL^{-1} bovine insulin (I6634, Sigma Aldrich) in 2 M acetic acid supplemented with 500 mM NaCl was placed in a water bath kept at 50 °C to induce formation of amyloid-like insulin fibrils. Aliquots of 100 μL were withdrawn at different time-points and mixed with 2 μL of the LCO stock solution (15 μM) or 2 μL of a ThT stock solution (15 μM). The fibrillation was also performed having 300 nM of LCO present during the fibrillation event. The samples were prepared in micro-titer plates and incubated for 10 min at room temperature. The emission spectra were recorded as described above.

LCO staining and spectral analysis

Cryosections (20 μm) of human brain tissue with AD pathology were fixed with ice cold acetone for 10 min at –20 °C and then allowed to dry. The sections were incubated with PBS for 10 min and then stained for 30 min at RT with t-HTAA, q-HTAA, q-FTAA, p-HTAA, p-FTAA, hx-HTAA, hx-FTAA, h-HTAA or h-FTAA. All probes were diluted 1 : 500 in PBS from a 1.5 mM stock. After rinsing with PBS three times, the sections were mounted with Dako fluorescence mounting medium (Dako Cytomation, Glostrup, Denmark). The medium was allowed to solidify for three hours before the rims were sealed with nail polish. Fluorescence and spectral images were collected with a Zeiss Axioplan epifluorescence microscope (Carl Zeiss, Jena, Germany) or a Leica DM6000 B fluorescence microscope (Leica, Wetzlar, Germany) equipped with a SpectraCube module (Applied Spectral Imaging, Migdal Ha-Emek, Israel). Bandpass filters 405/30 (LP450), 470/40 (LP515) and 546/12 (LP590) were used for the Zeiss microscope and bandpass filters 405/40 (LP455), 436/10 (LP475), 480/20 (LP 515) and 535/50 (LP590) were used for the Leica microscope. The emission profile of each LCO was obtained by collecting the emission spectrum for 7–8 regions of interest in five Aβ plaques and five tau tangles, respectively, using the above mentioned excitation wavelengths and the same exposure time for the two protein entities. Computational analyses were performed with the SpectraView 3.0 EXPO software (Applied Spectral Imaging), which is a program that renders it possible not only to obtain emission spectra for each excitation wavelength but also to merge two different excitations into one resulting emission spectrum. This operation was performed after exciting p-FTAA, hx-FTAA, h-HTAA and h-FTAA at 405 and 546 nm, and hx-HTAA at 405 and 535 nm. The same thing could not be done with t-HTAA, q-HTAA, q-FTAA or p-HTAA since their emission at 535 or 546 nm was almost nonexistent. The double-excitation emission spectra were used to make ratio plots for each LCO and determine their capability to spectrally separate Aβ plaques and tau tangles.

Immunostaining with antibodies

Cryosections of human Alzheimer's diseased brain were fixed with 4% PFA for 15 min, washed in PBS and then incubated in blocking buffer (PBS with 0.1% triton x-100 and 2% BSA) for 30 min. Aβ

plaques and NFTs were visualized by using monoclonal mouse anti-Aβ antibody (1 : 200, Mabtech, Nacka Strand, Sweden) diluted in PBS and monoclonal mouse anti-phosphorylated tau antibody AT8 (1 : 100, Pierce Endogen, Rockford, IL, USA) diluted in blocking buffer. Both antibodies were incubated overnight at 4 °C. The sections were washed with PBS (Mabtech) or blocking buffer (AT8) and then incubated with secondary Alexa Fluor 594-conjugated goat anti-mouse antibody (1 : 500 (Mabtech) or 1 : 400 (AT8), Molecular Probes, Eugene, OR, USA) for 30 min at RT. After washing, the sections were mounted with Dako mounting medium (Dako) for fluorescence and analysed by using a Zeiss Axioplan epifluorescence microscope (Carl Zeiss).

Abbreviations

CR	Congo red
ThT	Thioflavin T
LCPs	Luminescent conjugated polythiophenes
LCOs	Luminescent conjugated oligothiophenes
AD	Alzheimer's disease
Aβ	amyloid β
NFTs	neurofibrillary tangles;

Acknowledgements

Our work is supported by the Swedish Foundation for Strategic Research (K.P.R.N, P.H. T.K.), the Knut and Alice Wallenberg foundation (K.P.R.N, P.H.), and European Union FP7 HEALTH (Project LUPAS, P.H., K.P.R.N., A.Å, J.M., S.N.). K.P.R.N is financed by an ERC Starting Independent Researcher Grant (Project: MUMID) from the European Research Council and P.H. is a Swedish Royal Academy of Science Research Fellow sponsored by a grant from the Knut and Alice Wallenberg Foundation. We would also like to thank Prof. David M. Holztman, Prof. Nigel Cairns and the Knight Alzheimer's Disease Research Center (NIH grants P50AG05681 and 5PO1-AG03991) Washington University (St. Louis, MO, USA) for supplying us with human brain tissue and Mikael Lindgren for illuminating discussions on optical spectroscopy. A generous gift from Astrid and Georg Olsson is also gratefully acknowledged. T.K., R.A.S, L.B.G.J are enrolled in the doctoral program Forum Scientum.

References

1 F. Chiti and C. M. Dobson, *Annu. Rev. Biochem.*, 2006, **75**, 333–366.
2 L. C. Serpell, M. Sunde and C. C. Blake, *Cell. Mol. Life Sci.*, 1997, **53**, 871–887.
3 M. Sunde and C. Blake, *Adv. Protein Chem.*, 1997, **50**, 123–159.
4 L. C. Serpell, M. Sunde, M. D. Benson, G. A. Tennent, M. B. Pepys and P. E. Fraser, *J. Mol. Biol.*, 2000, **300**, 1033–1039.
5 P. Ladewig, *Nature*, 1945, **156**, 81–82.
6 W. E. Klunk, J. W. Pettegrew and D. J. Abraham, *J. Histochem. Cytochem.*, 1989, **37**, 1273–1281.
7 D. P. Steensma, *Arch. Pathol. Lab. Med.*, 2001, **125**, 250–252.
8 P. S. Vassar and C. F. Culling, *Arch. Pathol.*, 1959, **68**, 487–498.
9 H. LeVine, 3rd, *Protein Sci.*, 1993, **2**, 404–410.
10 H. LeVine, 3rd, *Methods Enzymol.*, 1999, **309**, 274–284.
11 M. Groenning, *J. Chem. Biol.*, 2010, **3**, 1–18.
12 E. D. Eanes and G. G. Glenner, *J. Histochem. Cytochem.*, 1968, **16**, 673–677.
13 L. Bonar, A. S. Cohen and M. M. Skinner, *Proc. Soc. Exp. Biol. Med.*, 1969, **131**, 1373–1375.
14 J. D. Sipe and A. S. Cohen, *J. Struct. Biol.*, 2000, **130**, 88–98.
15 R. Khurana, V. N. Uversky, L. Nielsen and A. L. Fink, *J. Biol. Chem.*, 2001, **276**, 22715–22721.
16 L. Bousset, V. Redeker, P. Decottignies, S. Dubois, P. Le Marechal and R. Melki, *Biochemistry*, 2004, **43**, 5022–5032.
17 J. Hardy and D. J. Selkoe, *Science*, 2002, **297**, 353–356.
18 D. M. Walsh, I. Klyubin, J. V. Fadeeva, W. K. Cullen, R. Anwyl, M. S. Wolfe, M. J. Rowan and D. J. Selkoe, *Nature*, 2002, **416**, 535–539.
19 J. L. Tomic, A. Pensalfini, E. Head and C. G. Glabe, *Neurobiol. Dis.*, 2009, **35**, 352–358.
20 K. P. R. Nilsson, A. Herland, P. Hammarström and O. Inganäs, *Biochemistry*, 2005, **44**, 3718–3724.
21 K. P. R. Nilsson, P. Hammarström, F. Ahlgren, A. Herland, E. A. Schnell, M. Lindgren, G. T. Westermark and O. Inganäs, *ChemBioChem*, 2006, **7**, 1096–1104.
22 K. P. R. Nilsson, A. Åslund, I. Berg, S. Nyström, P. Konradsson, A. Herland, O. Inganäs, F. Stabo-Eeg, M. Lindgren, G. T. Westermark, L. Lannfelt, L. N. Nilsson and P. Hammarström, *ACS Chem. Biol.*, 2007, **2**, 553–560.
23 C. J. Sigurdson, K. P. R. Nilsson, S. Hornemann, G. Manco, M. Polymenidou, P. Schwarz, M. Leclerc, P. Hammarström, K. Wuthrich and A. Aguzzi, *Nat. Methods*, 2007, **4**, 1023–1030.
24 O. Philipson, P. Hammarström, K. P. R Nilsson, E. Portelius, T. Olofsson, M. Ingelsson, B. T. Hyman, K. Blennow, L. Lannfelt, H. Kalimo and L. N. G. Nilsson, *Neurobiol. Aging*, 2009, **30**, 1393–1405.
25 K. P. R. Nilsson, K. Ikenberg, A. Åslund, S. Fransson, P. Konradsson, C. Rocken, H. Moch and A. Aguzzi, *Am. J. Pathol.*, 2010, **176**, 563–574.
26 A. Åslund, C. J. Sigurdson, T. Klingstedt, S. Grathwohl, T. Bolmont, D. L. Dickstein, E. Glimsdal, S. Prokop, M. Lindgren, P. Konradsson, D. M. Holtzman, P. R. Hof, F. L. Heppner, S. Gandy, M. Jucker, A. Aguzzi, P. Hammarström and K. P. R. Nilsson, *ACS Chem. Biol.*, 2009, **4**, 673–684.
27 A. Åslund, K. P. R. Nilsson and P. Konradsson, *J. Chem. Biol.*, 2009, **2**, 161–175.
28 T. Klingstedt and K. P. R. Nilsson, *Biochim. Biophys. Acta, Gen. Subj.*, 2011, **1810**, 286–296.
29 C. J Sigurdson, K. P. R. Nilsson, S. Hornemann, M. Heikenwalder, G. Manco, P. Schwarz, D. Ott, T. Rülicke, P. P. Liberski, C. Julius, J. Falsig, L. Stitz, K. Wüthrich and A. Aguzzi, *Proc. Natl. Acad. Sci. U. S. A.*, 2009, **106**, 304–309.
30 I. Berg, K. P. R. Nilsson, S. Thor and P. Hammarström, *Nat. Protoc.*, 2010, **5**, 935–944.
31 K. P. R. Nilsson, S. Joshi-Barr, O. Winson and C. J. Sigurdson, *J. Neurosci.*, 2010, **30**, 12094–12102.
32 A. Lord, O. Philipson, T. Klingstedt, G. Westermark, P. Hammarström, K. P. R. Nilsson and L. N. Nilsson, *Am. J. Pathol.*, 2011, **178**, 2286–2298.
33 S. W. Schultz, K. P. R. Nilsson and G. T. Westermark, *PLoS One*, 2011, **6**, e20221.
34 V. Mahajan, T. Klingstedt, R. Simon, K. P. R Nilsson, A. Thueringer, K. Kashofer, J. Haybaeck, H. Denk, P. M. Abuja and K. Zatloukal, *Gastroenterology*, 2011, **141**, 1080–1090.
35 P. Hammarström, R. Simon, S. Nyström, P. Konradsson, A. Åslund and K. P. R. Nilsson, *Biochemistry*, 2010, **49**, 6838–6845.
36 A. Åslund, A. Herland, P. Hammarström, K. P. R. Nilsson, B. H. Jonsson, O. Inganäs and P. Konradsson, *Bioconjugate Chem.*, 2007, **18**, 1860–1868.
37 E. S. Voropai, K. N. Kaplevskii, A. A. Maskevich, V. I. Stepuro, O. I. Pavarova, I. M. Kuznetsova, K. K. Turoverov, A. L. Fink and V. N. Uverskii, *J. Appl. Spectrosc.*, 2003, **70**, 868–874.
38 F. Stabo-Eeg, M. Lindgren, K. P. R. Nilsson, O. Inganäs and P. Hammarström, *Chem. Phys.*, 2007, **336**, 12–126.
39 C. Wu, M. T. Bowers and J. E. Shea, *Biophys. J.*, 2011, **100**, 1316–1324.
40 C. Wu, H. Lei, W. Zhang and Y. Duan, *J. Am. Chem. Soc.*, 2007, **129**, 1225–1232.
41 M. Biancalana, K. Makabe, A. Koide and S. Koide, *J. Mol. Biol.*, 2009, **385**, 1052–1063.
42 A. Herland, P. Björk, P. R. Hania, I. G. Scheblykin and O. Inganäs, *Small*, 2007, **3**, 318–325.

43 D. A. Yushchenko, J. A. Fauerbach, S. Thirunavukkuarasu, E. A. Jares-Erijman and T. M. Jovin, *J. Am. Chem. Soc.*, 2010, **132**, 7860–7861.
44 B. Vestergaard, M. Groenning, M. Roessle, J. S. Kastrup, M. van de Weert, J. M. Flink, S. Frokjaer, M. Gajhede and D. I. Svergun, *PLoS Biol.*, 2007, **5**, e134.
45 L. Qin, J. Vastl and J. Gao, *Mol. BioSyst.*, 2010, **6**, 1791–1795.
46 M. Lindgren, K. Sörgjerd and P. Hammarström, *Biophys. J.*, 2005, **88**, 4200–4212.
47 L. S. Wolfe, M. F. Calabrese, A. Nath, D. V Blaho, A. D. Miranker and Y. Xiong, *Proc. Natl. Acad. Sci. U. S. A.*, 2010, **107**, 16863–16868.
48 M. Biancalana and S. Koide, *Biochim. Biophys. Acta.*, 2010, **1804**, 1405–1412.
49 A. L. Cloe, J. P. Orgel, J. R. Sachleben, R. Tycko and S. C. Meredith, *Biochemistry*, 2011, **50**, 2026–2039.
50 J. Z. Wang and L. Liu, *Prog. Neurobiol.*, 2008, **85**, 148–175.
51 H. E. Gottlieb, V. Kotlyar and A. Nudelman, *J. Org. Chem.*, 1997, **62**, 7512–7515.

